crystals

MDPI

Article

Preparation of NaA Zeolite from High Iron and Quartz Contents Coal Gangue by Acid Leaching—Alkali Melting Activation and Hydrothermal Synthesis

Deshun Kong [1,2] and Rongli Jiang [1,*]

[1] School of Chemical Engineering and Technology, China University of Mining and Technology, Xuzhou 221016, China; LB19040009@cumt.edu.cn
[2] Guizhou Provincial Key Laboratory of Coal Clean Utilization, School of Chemistry and Materials Engineering, Liupanshui Normal University, Liupanshui 553004, China
* Correspondence: ronglij@cumt.edu.cn

Abstract: In this study, NaA zeolite was successfully synthesized from coal gangue with high contents of iron and quartz as the main raw material. The results show that most iron ions can be removed from coal gangue after calcination at 700 °C for 2 h, leaching in hydrochloric acid with a mass fraction of 20% for 7 h and a liquid-solid ratio of 3.5:1. When *m* (acid leached residue of calcined gangue):*m* (Na_2CO_3) = 1.1 and melting at 750 °C for 2 h, the quartz and other aluminosilicates turn into nepheline, which dissolve in water. Finally, the optimum conditions of synthesis NaA zeolite are as follows: $n(SiO_2)/n(Al_2O_3)$ = 2.0, $n(Na_2O)/n(SiO_2)$ = 2.1, $n(H_2O)/n(Na_2O)$ = 55, aging at 60 °C for 2 h, and crystallization at 94 °C for 4 h. This shows that the high iron and quartz contents coal gangue can be used for the synthesis of NaA zeolite.

Keywords: high iron and quartz contents coal gangue; acid leaching; alkali melting; hydrothermal reaction; NaA zeolite

Citation: Kong, D.; Jiang, R. Preparation of NaA Zeolite from High Iron and Quartz Contents Coal Gangue by Acid Leaching—Alkali Melting Activation and Hydrothermal Synthesis. *Crystals* **2021**, *11*, 1198. https://doi.org/10.3390/cryst11101198

Academic Editor: Sergio Brutti

Received: 12 September 2021
Accepted: 30 September 2021
Published: 3 October 2021

1. Introduction

Coal gangue is the main discharged waste of the coal industry [1,2]. The arbitrary stacking of it seriously influences the safety of the ecological environment [3,4]. Recently, the development and utilization of coal gangue as a kind of new resource has gained interest [5–7]. Many products have been prepared from coal gangue, but the common utilization methods of coal gangue are as power plant fuel [8] and to prepare building materials [9], including brick [10], cement clinker products [11] and other products. The utilization technology level is lower and the industrial added value is not high. On the other hand, zeolite synthesis often uses cheap minerals or waste, which can save the cost of raw materials. Coal gangue can be used as raw material for preparing zeolites [12,13]. In recent years, researchers have noticed the great potential of coal gangue in zeolite synthesis [14–16].

Zeolites are micropore and mesoporous hydrated aluminosilicates containing alkali elements, alkaline earth metals, or other cations, whose structure is built up with a framework of tetrahedral molecules, which are linked with shared oxygen atoms [17]. Due to their unique properties, zeolites have been used in many fields, such as in agriculture [18], chemical technology [19], oil refining [20], and others for their porous characteristics, ion-exchange properties, and catalytic performance [21]. Many studies have succeeded in the conversion of low iron-bearing coal gangue into synthetic zeolites [22–24]. However, coal gangue with high iron content is a kind of material with poor quality. It is difficult to synthesize high quality zeolite because iron ions will affect the whiteness and performance of the products, therefore, there are only a few studies concerning what happens in the transformation process of the whole NaA zeolite preparation from high iron content coal gangue.

In this work, coal gangue is firstly calcined and then leached by acid to remove most of the iron ions; at the same time, there is very low chemical activity of kaolinite and quartz in the coal gangue, which are necessary to be activated before synthesizing zeolite. However, the quartz in gangue is difficult to activate by heating, which will directly enter the zeolite products [25]. In zeolite synthesis, the alkali melting method, as an activator for the formation of soluble aluminate and silicate [26–28], is adopted to activate the materials richly with inert silica or alumina in the presence of alkali. In the process, the acid-leached residue of coal gangue is activated absolutely by Na_2CO_3 powder at 750 °C for 2 h after calcination of the coal gangue powder at 700 °C for 2 h, and leaching in 20% hydrochloric acid at 90 °C for 7 h under stirring. The NaA zeolite is obtained following aging and hydrothermal synthesis. For further discussion of the mechanism of phase transformations, the gangue, acid-leached residue, alkali-melted intermediate products, and the NaA zeolite, which are prepared under different conditions, are detected by XRD; the phase transformation laws are obtained; and the suitable technological conditions for preparing NaA zeolite from high iron and quartz contents coal gangue are determined.

2. Experimental

2.1. Materials

The coal gangue comes from Wangjiazhai Coal Mine in Liupanshui, Guizhou Province, China, which is made into powder of less than 200 mesh. $NaAiO_2$ and Na_2CO_3 are analytically pure (AR), Tianjin city Beichen Founder Reagent Factory; Tianjin, China; NaOH is AR, Tianjin Zhiyuan Chemical Reagents Co., Ltd. Tianjin, China; and hydrochloric acid is AR, Chongqing Chuandong Chemical Co., Ltd. Chongqing, China.

2.2. Technological Process

The coal gangue is calcined at 700 °C for 2 h and then leached by 20% (in mass) hydrochloric acid; the liquid to solid ratio is 3.5:1 (volume/mL:mass/g) at 90 °C for 7 h; and the acid leached residue is obtained after filtering and drying, and then the residue is mixed with sodium carbonate at the ratio of *m* (acid leaching residue):*m* (Na_2CO_3) = 1.1, melting at 750 °C for 2 h in the muffle, by adjusting the reacting proportion and aging; the hydrothermal crystallization is completed under the stirring condition of 94 °C for several hours, and NaA powder zeolite is obtained after washing and drying.

The preparation process of NaA zeolites from high-iron content coal gangue is shown in Figure 1.

2.3. Characterization

TD-2500 type X-ray diffraction instrument (XRD, China) was used for CuK_α (λ for K_α = 1.54059 Å), 2θ = 3° (min)–65° (max), with a step width of 0.04°. The major chemical elemental compositions were detected by Thermo Electron ARL9900XP+ type X-ray fluorescence spectrometer (XRF, Massachusetts, USA). The morphology of the products was detected by Zeiss evo18 type scanning electron microscope (SEM, Jena, Germany).

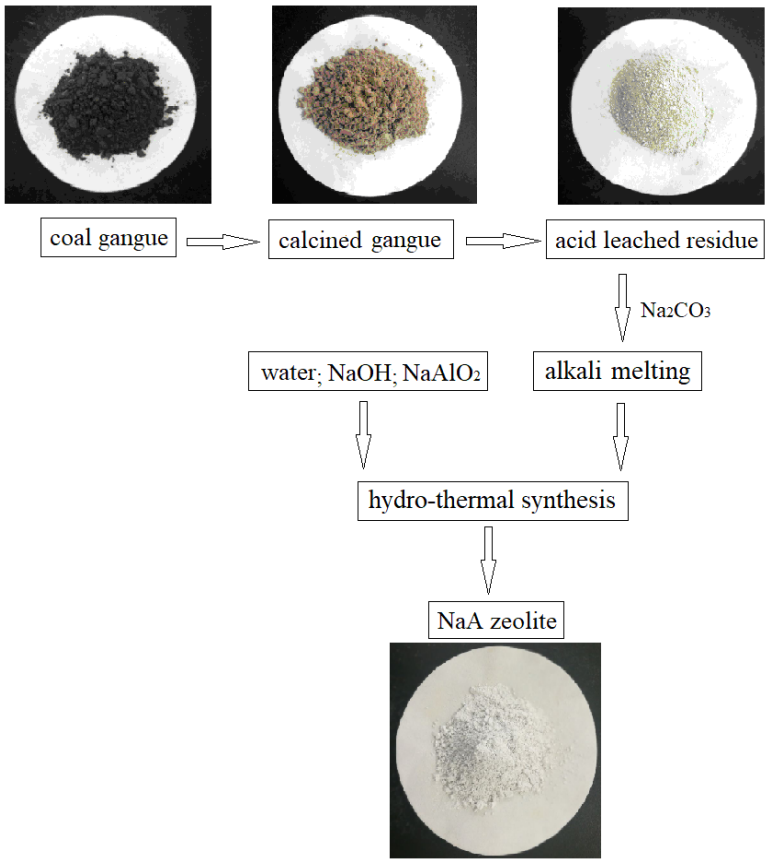

Figure 1. Process flow chart of preparing NaA zeolite from high iron coal gangue.

3. Results and Discussions

3.1. Major Chemical Elements Analysis of Coal Gangue and the Acid Leached Residue

The raw coal gangue and the acid leached residue are dried at 105 °C for 12 h [29], the main compositions are shown in Table 1.

Table 1. Main compositions of coal gangue and the acid-leaching residue/*wt* %.

Compositions	Gangue	Residue
SiO_2	42.18	83.12
Al_2O_3	20.43	10.50
Fe_2O_3	15.36	0.99
K_2O	1.24	1.04
Na_2O	0.40	0.38
CaO	2.95	0.04
MgO	1.61	0.19
MgO	1.66	2.77
TiO_2	0.25	0.04
MnO	0.54	0.03
S	0.30	0.06
FC and other ignition loss	13.08	0.84

We can see from Table 1 that the main compositions of the gangue are silicon, aluminum, and iron; obviously the iron element content is too high, which will affect the properties of the NaA product, so it must be removed. After acid leaching by hydrochloric acid, the major chemical elements of the residue are silicon and aluminum; the contents of other elements are low, $n(SiO_2)/n(Al_2O_3)$ = 13.46, compared with NaA zeolite ($n(SiO_2)/n(Al_2O_3)$ = 2.0), so it is necessary for $NaAlO_2$ to adjust the $n(SiO_2)/n(Al_2O_3)$ ratio of the system.

The morphology analyses of the gangue powder, calcined gangue, and residue are shown in Figures 2–5.

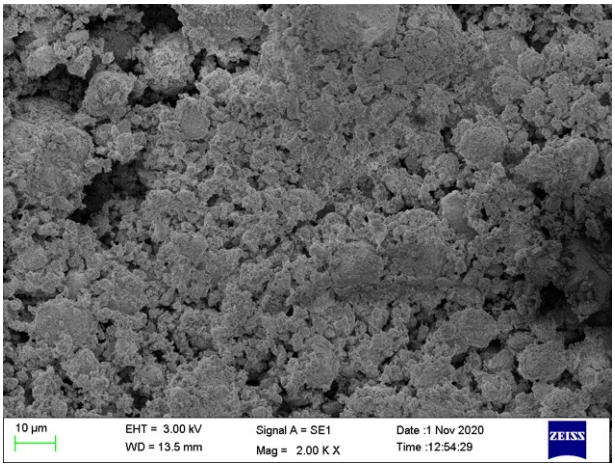

Figure 2. SEM image of raw gangue powder.

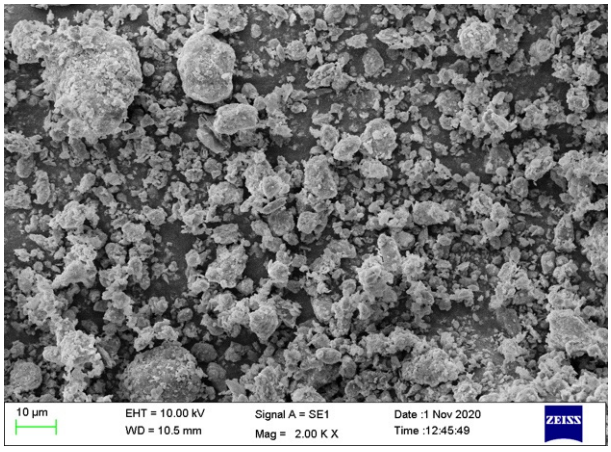

Figure 3. SEM image of 700 °C calcined gangue.

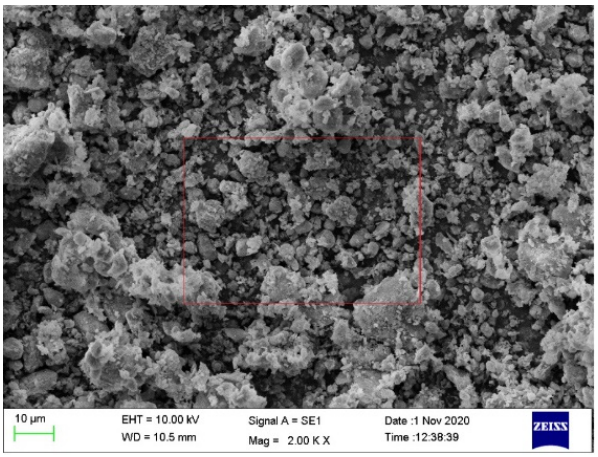

Figure 4. SEM image of acid-leached residue.

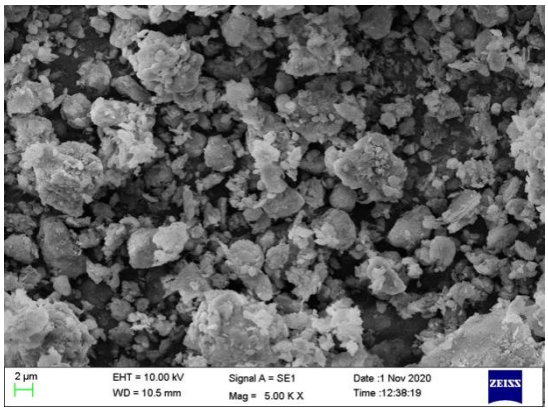

Figure 5. The SEM image of acid-leached residue (taken from Figure 4).

As seen, the particles of raw gangue powder are relatively uniform at 15–20 µm or larger in Figure 2; after calcination, the particle size decreases and fragments appear. After acid leaching, the number of flaky debris increases significantly. Most particle sizes are less than 5 µm, which is due to the overflow of water in coal gangue after calcination. Moreover, kaolinite decomposes into amorphous Al_2O_3 and SiO_2, at 700 °C; most of the iron content and part of Al_2O_3 are dissolved in the acid solution.

In order to observe the particle morphology of acid-leached residue more clearly, we enlarged a region in Figure 4 and marked it red, then got Figure 5. Figure 5 shows that many small particles become smoother, this is because the edges and corners of some particles are worn off by stirring, which makes the raw material more fragmented, so it is conducive to the alkali-melting reaction in the next step.

3.2. Phase Analysis of the Residue and Activation Product

Figure 6 shows that the crystal substances in the coal gangue mainly contain kaolinite and quartz, as well as a small amount of pyrite and siderite. Table 1 shows that the iron element content in the coal gangue is very high, but the diffraction peaks of iron-containing materials are very weak in Figure 6, which indicates that the iron materials are amorphous. After calcination, kaolinite turns into metakaolin, its crystal structure is destroyed, and the carbon in coal gangue is removed.

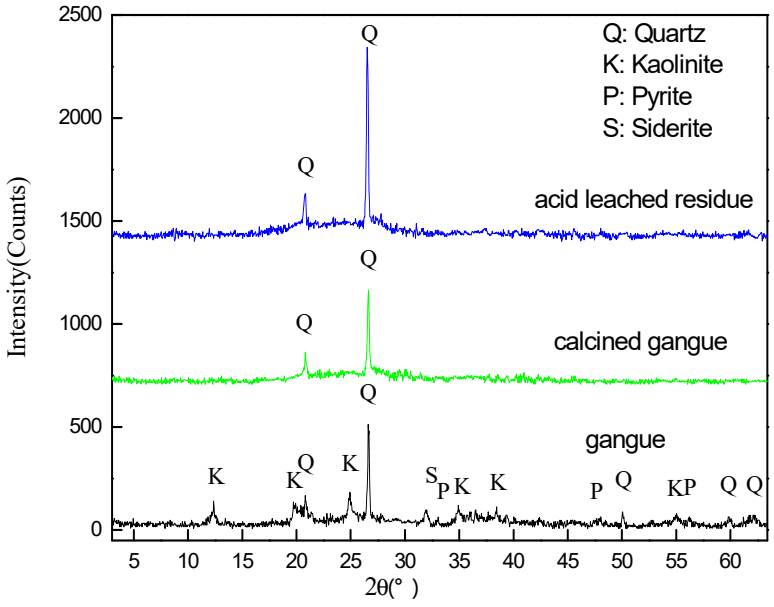

Figure 6. XRD patterns of coal gangue powder at 750 °C, calcined powder, and acid-leached residue.

The quartz is inert and it is difficult for it to participate in the crystallization reaction directly, so it must to be activated before the crystallization reaction. Therefore, according to the mass ratio of *m* (acid leached residue):*m* (sodium carbonate) = 1:1.1, after mixing the sodium carbonate evenly with the residue, the mixture is melted at 750 °C for 2 h, then the melted powder is analyzed by XRD and added to the water to be fully grinded then filtered; the XRD analyses are shown in Figure 7.

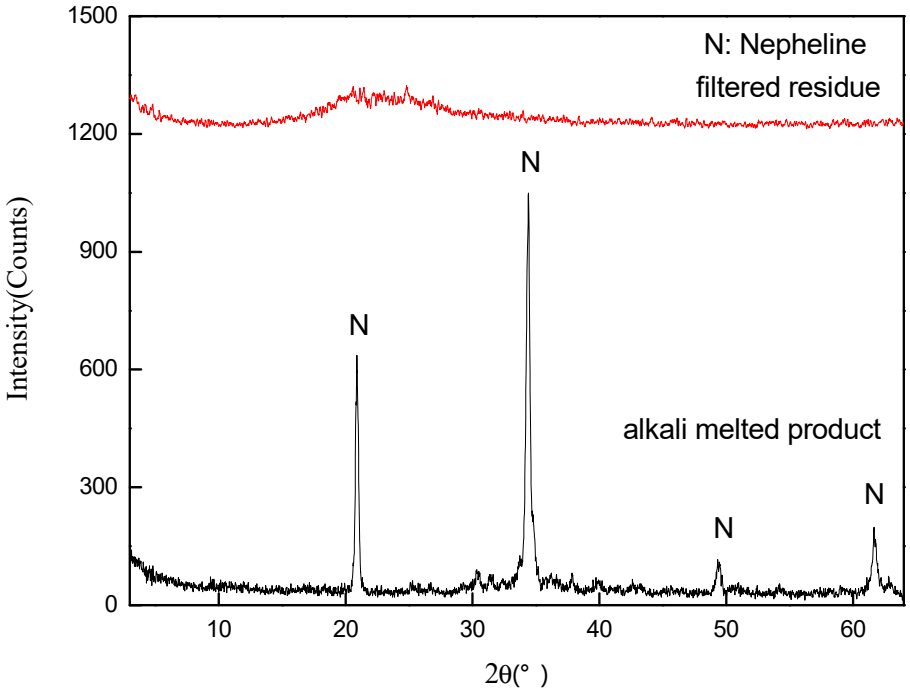

Figure 7. XRD spectra of alkali-melted product and its water washing filter residue.

Figure 7 shows that the alkali melted product is mainly nepheline (nepheline, PDF card number: 76-1733), its chemical formula is $NaAlSiO_4$, and the main reaction equations of acid-leached filter residue with sodium carbonate at 750 °C are as follows:

$$Na_2CO_3 + SiO_2 = Na_2SiO_3 + CO_2\uparrow \quad (1)$$

$$Al_2O_3{\cdot}2SiO_2 + Na_2CO_3 = 2NaAlSiO_4 + CO_2\uparrow \quad (2)$$

The metakaolin and quartz, which contain silicon and aluminum substances, can react with Na_2CO_3 at 750 °C, and nepheline can dissolve in water, so it can be used as silicon and aluminum sources to synthesize NaA zeolite. Therefore, this method can completely activate the quartz in the acid-leached residue; it not only takes full advantage of the silicon and aluminum sources in the residue but also avoids the quartz entering NaA zeolite products, which increases the quality of NaA products, so the soluble intermediate product $NaAlSiO_4$ with higher chemical activity is beneficial to the hydrothermal crystallization reaction.

The rest filter residue contains amorphous SiO_2 and Al_2O_3, they both have high chemical activity and can react with sodium aqueous solution in the hydrothermal synthesis period; the reactions are as follows:

$$SiO_2 + 2NaOH = Na_2SiO_3 + H_2O \quad (3)$$

$$Al_2O_3 + 2NaOH = 2NaAlO_2 + H_2O \quad (4)$$

Na_2SiO_3 and $NaAlO_2$ can be used as the active silicon source and aluminum sources to synthesis NaA zeolite. Because the synthesis of NaA zeolite is closely related to

$n(SiO_2)/n(Al_2O_3)$, $n(Na_2O)/n(SiO_2)$, $n(H_2O)/n(Na_2O)$, aging temperature, and crystallization time, so the experiments focused on these five factors.

3.3. Effects of $n(SiO_2)/n(Al_2O_3)$ on the Product Phase

Setting the reaction system to $n(H_2O)/n(Na_2O)$ = 50; $n(Na_2O)/n(SiO_2)$ = 1.2; aging at 50 °C for 1 h; crystallization at 94 °C for 4 h,; and changing $n(SiO_2)/n(Al_2O_3)$ = 1.0, 1.5, 2.0, and 2.5 respectively, after hydrothermal crystallization reaction, the XRD analyses are shown in Figure 8.

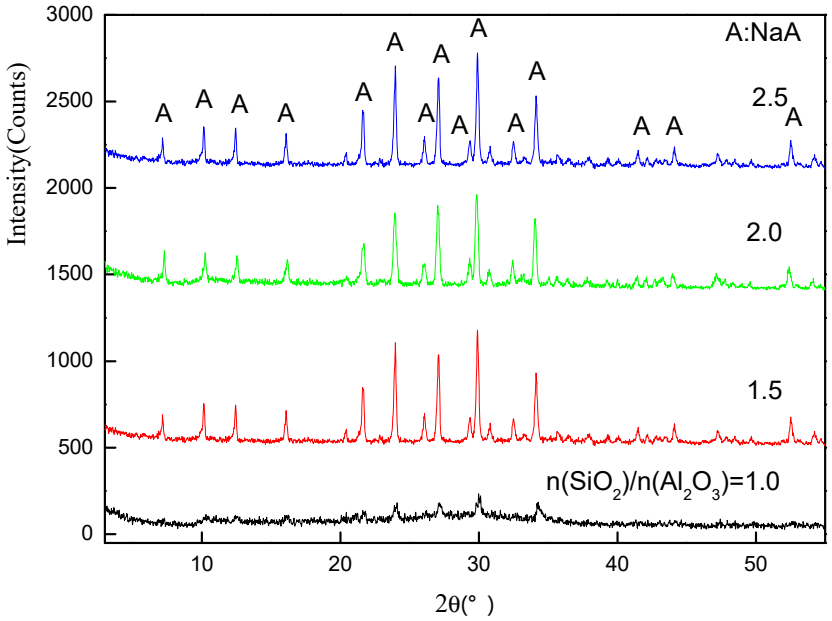

Figure 8. Effect of $n(SiO_2)/n(Al_2O_3)$ on the phase.

Figure 8 shows when $n(SiO_2)/n(Al_2O_3)$ = 1.0, the diffraction peak intensity of the product is very low, this is because the crystallinity and the zeolite type highly depend on the $n(SiO_2)/n(Al_2O_3)$ ratios [30–34]; when $n(SiO_2)/n(Al_2O_3)$ = 1.0 or 1.5, they deviate from the target NaA zeolite product $n(SiO_2)/n(Al_2O_3)$ = 2.0, which is not conducive to the nucleation and growth of zeolite; when $n(SiO_2)/n(Al_2O_3)$ = 2.0, the diffraction intensity increases. The search result shows that the final product is NaA zeolite (PDF card number: 39-0223), there is a further increase of $n(SiO_2)/n(Al_2O_3)$ = 2.5, and the diffraction intensity also increases. If the $n(SiO_2)/n(Al_2O_3)$ ratio is too high, the higher $n(SiO_2)/n(Al_2O_3)$ ratio products such as NaX and NaP zeolites may appear; in order to take full use of the silicon and aluminum components, $n(SiO_2)/n(Al_2O_3)$ = 2.0 is selected.

3.4. Effects of $n(Na_2O)/n(SiO_2)$ on the Phase

Setting the reaction system to $n(SiO_2)/n(Al_2O_3)$ = 2.0; $n(H_2O)/n(Na_2O)$ = 60; aging at 50 °C for 1 h; crystallization at 94 °C for 4 h; and changing $n(Na_2O)/n(SiO_2)$ = 1.2, 1.7, 1.9, and 2.1, respectively, after finishing reactions, the XRD analyses of the products are shown in Figure 9.

In Figure 9, the intensity of these spectra is high and their shapes are similar. This is because $n(Na_2O)/n(SiO_2)$ works together with $n(H_2O)/n(Na_2O)$; they change the alkalinity of the solution and affect the growth rate of zeolite. When the $n(Na_2O)/n(SiO_2)$ ratio is larger, the system alkalinity is higher, which promotes the dissolution rate of the materials and the growth rate of NaA zeolite crystal; when $n(Na_2O)/n(SiO_2)$ = 2.1, the intensity of diffraction peaks is high and there are no other miscellaneous crystals, so $n(Na_2O)/n(SiO_2)$ = 2.1 is selected.

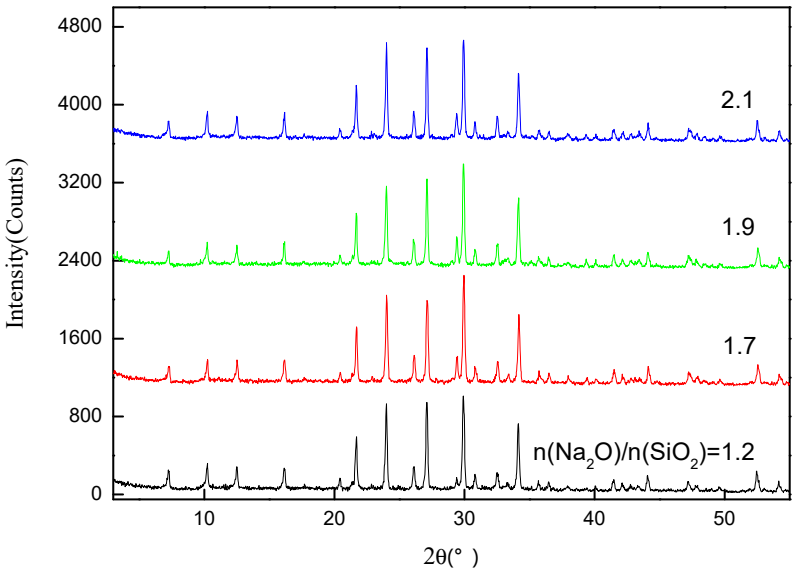

Figure 9. Effects of $n(Na_2O)/n(SiO_2)$ on the phase.

3.5. Effects of n(H2O)/n(Na2O) on the Phase

Setting the reaction system to $n(SiO_2)/n(Al_2O_3)$ = 2.0; $n(Na_2O)/n(SiO_2)$ = 1.7; the aging temperature as 50 °C; aging time as 2 h; crystallization at 94 °C for 4 h; and changing $n(H_2O)/n(Na_2O)$ = 50, 55, 60, and 65 respectively, after the reactions, the XRD analyses are shown in Figure 10.

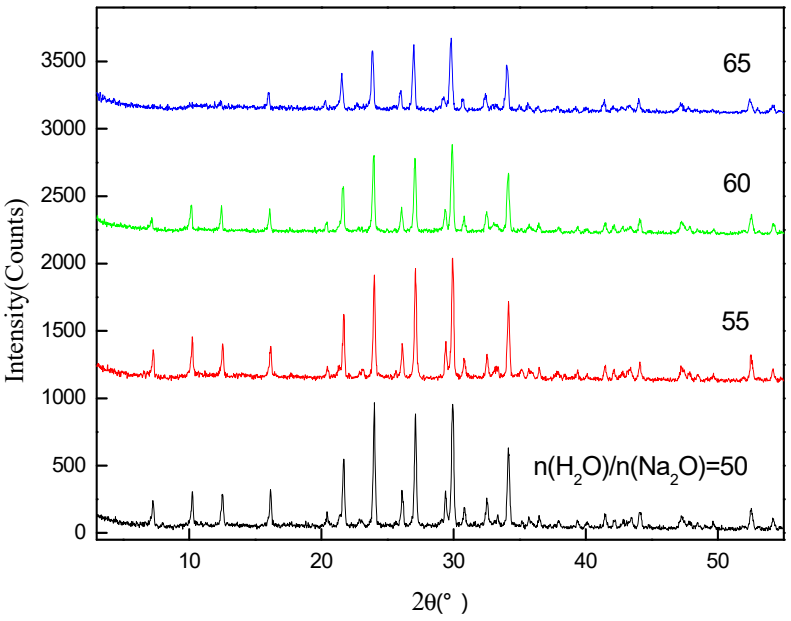

Figure 10. Effect of $n(H_2O)/n(Na_2O)$ on the phase.

We can see from Figure 10, as the value of $n(H_2O)/n(Na_2O)$ increases, the diffraction peak intensity decreases gradually. When $n(H_2O)/n(Na_2O)$ = 55, the intensity of the diffraction peaks are at maximum, and this is due to the high alkalinity concentration, which lead to large viscosity of the system and is not conducive to the mass transfer process, but is adverse to the dissolution of solid silicon and aluminum components in the system [35]. The reaction system cannot provide sufficient highly active raw material for crystal growth, which causes the intensity of the peaks to decrease, and so $n(H_2O)/n(Na_2O)$ = 55 is selected.

3.6. Effect of Aging Temperature on the Phase

Setting reaction system $n(SiO_2)/n(Al_2O_3) = 2.0$; $n(H_2O)/n(Na_2O) = 55$; $n(Na_2O)/n(SiO_2) = 2.1$; the aging time as 2 h; crystallization at 94 °C for 4 h; and changing aging temperature to 30 °C, 40 °C, 50 °C, and 60 °C respectively, after the crystallization reaction, the XRD analyses of the products are shown in Figure 11.

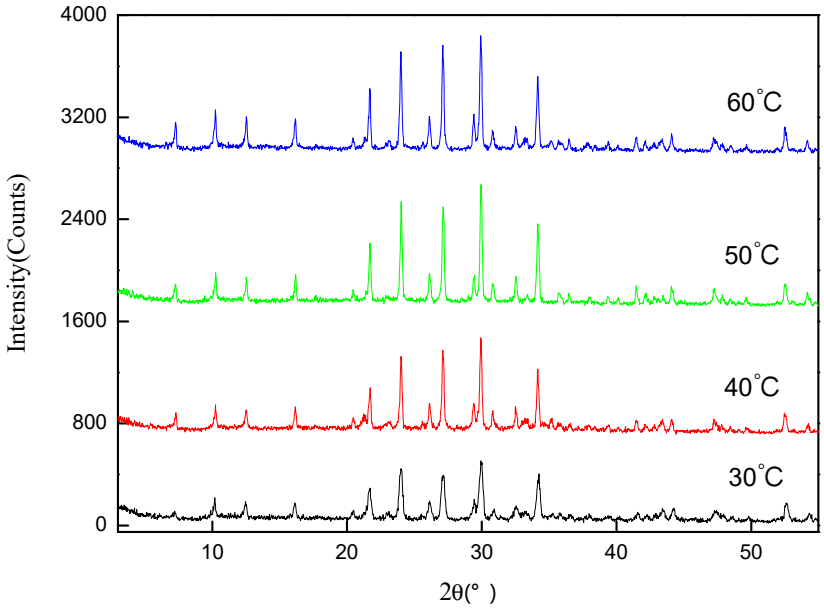

Figure 11. Effect of aging temperature on the phase.

The effect of aging temperature is reflected in the process of transforming the liquid sol into zeolite. It can be seen from Figure 11 that when the aging temperature is 30 °C or 40 °C, the intensity of diffraction peaks is low; when the aging temperature is 50 °C or 60 °C, the intensity is high, and this is because the low-temperature aging stage can improve the nucleation rate, reduce the grain size, and increase the number of crystals [36]. When the aging temperature is 50 °C or 60 °C, the raw materials can be fully dissolved and the nucleation will grow sooner, but if the aging temperature is too high, it will reduce the number of nucleation, so the proper aging temperature is 60 °C.

3.7. Effect of Crystallization Time on the Phase and Morphology

Setting reaction system $n(SiO_2)/n(Al_2O_3) = 2.0$; $n(H_2O)/n(Na_2O) = 65$; $n(Na_2O)/n(SiO_2) = 2.1$; aging at 60 °C for 2 h; crystallization temperature as 94 °C, and changing the crystallization time to 1 h, 2 h, 3 h, and 4 h respectively, after the reactions, the XRD patterns of the products are shown in Figure 12, and the SEM images are shown in Figures 13–16.

The crystallization time is particularly important for synthesis zeolites; it mainly affects their crystallinity. We can see from Figure 12, when the crystallization time is 1 h or 2 h, the intensity of the peaks is low; when the crystallization time is 1 h, just a small number of little NaA crystals begin to appear (Figure 13); most of the crystals are about 1 μm in size. With the extension of reaction time to 2–4 h, a large number of crystals begin to appear, the crystals are a regular cubic shape and the particle size is about 2 μm. At the same time, when the crystallization time is 4 h, the intensity of the peaks is relatively higher, which is due to the longer crystallization time that gives zeolite enough time to grow, so the crystallization reaction time is determined to be 4 h.

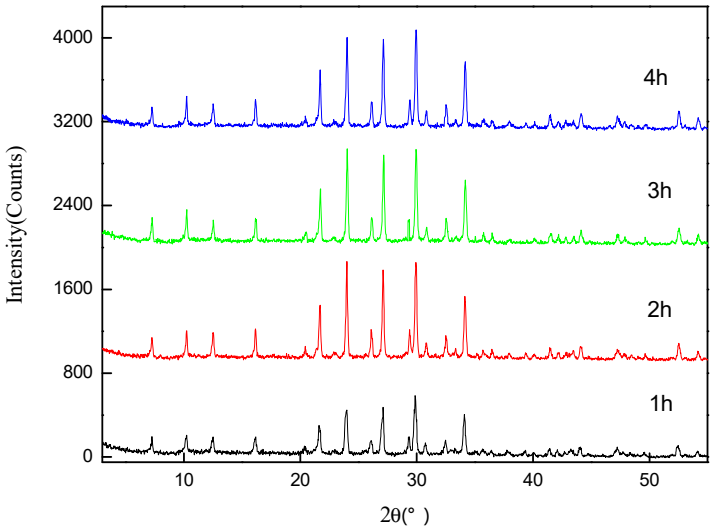

Figure 12. Effect of crystallization time on the phase.

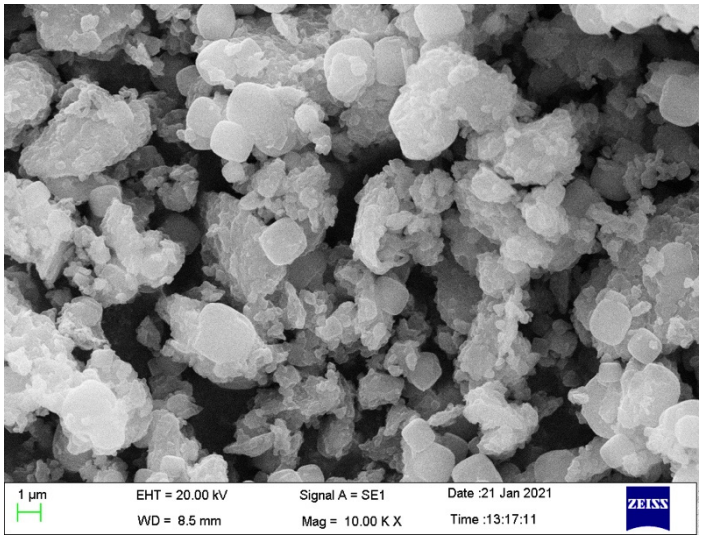

Figure 13. The crystallization time is 1 h.

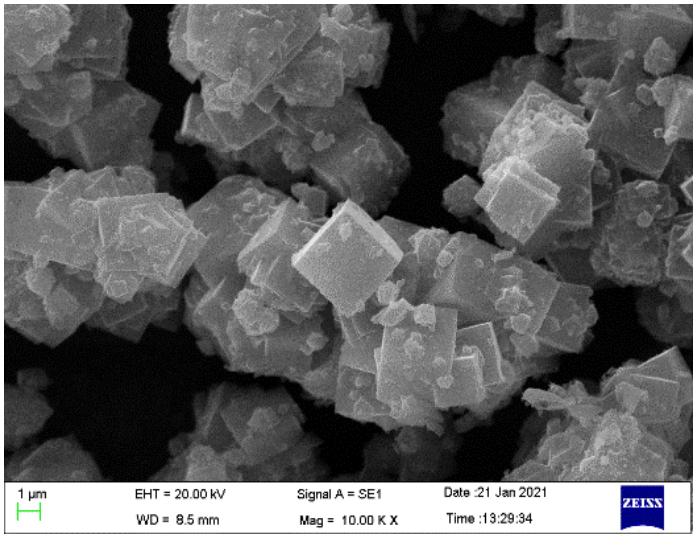

Figure 14. The crystallization time is 2 h.

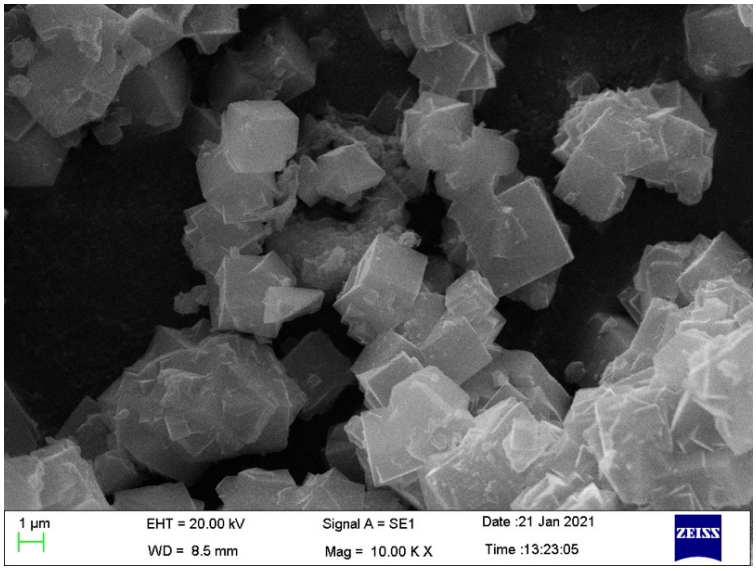

Figure 15. The crystallization time is 3 h.

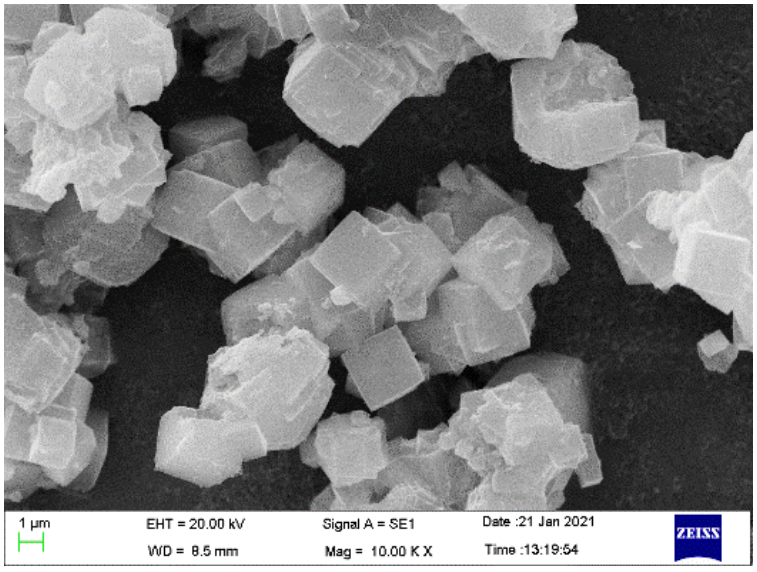

Figure 16. The crystallization time is 4 h.

3.8. XRD and SEM Analyses of the Product under Optimized Conditions

The product prepared under the above optimized conditions was detected by XRD and SEM; the results are shown in Figures 17 and 18.

After searching, the d values and 2 theta values are in good agreement with PDF card: 39-0223, so the product can be confirmed as NaA zeolite. As shown in Figure 17, the product is pure NaA zeolite, the diffraction peaks are sharp, and the intensity of the diffraction peaks are high, which indicates that the crystallinity of the product is high. Figure 18 shows that NaA zeolites prepared under the optimized conditions have regular cubic shapes and a uniform particle size of about 2.5 µm.

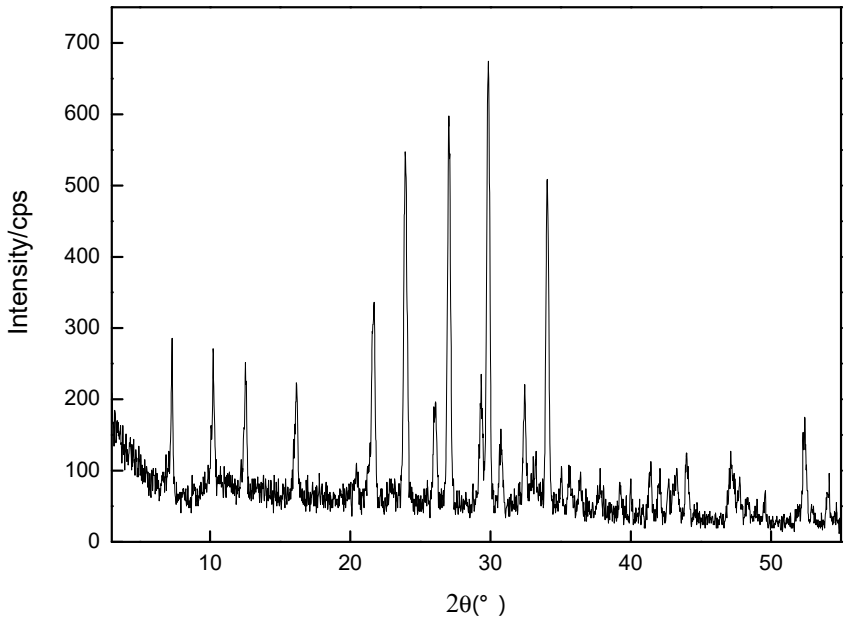

Figure 17. XRD spectra of the product under optimized conditions.

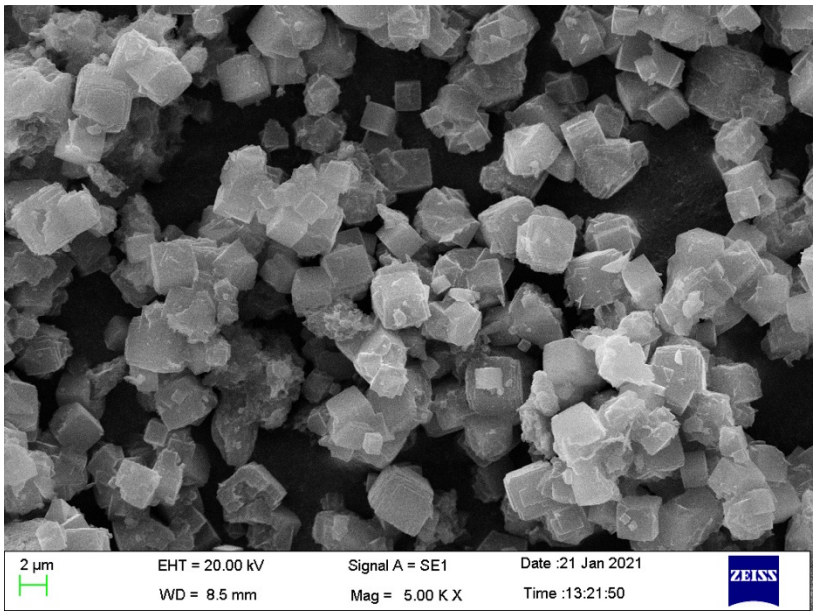

Figure 18. SEM photo of the product under optimized conditions.

3.9. Preparation Mechanism

The NaA zeolite is from high iron content coal gangue; many chemical reactions occurred in the process, in addition to the reactions mentioned above. Nepheline is produced by high temperature reaction and can be hydrolyzed under alkaline conditions. The equations are as follows:

$$2NaAlSiO_4 + 4NaOH = 2NaAlO_2 + 2Na_2SiO_3 + 2H_2O \quad (5)$$

$$SiO_2 + 2NaOH = Na_2SiO_3 + H_2O \quad (6)$$

$$Al_2O_3 + 2NaOH = 2NaAlO_2 + H_2O \quad (7)$$

The $NaAlSiO_4$ dissolves in NaOH solution to form $NaAlO_2$ and Na_2SiO_3, the amorphous SiO_2 in the residue reacts with NaOH solution to form Na_2SiO_3, and amorphous

Al_2O_3 in the residue reacts with NaOH solution to form $NaAlO_2$ [37–39]. In the silicate ions and aluminate ions system, the primary structural unit of silica–alumina zeolite skeleton is a silica–oxygen tetrahedron and alumina–oxygen tetrahedron, which are both called TO_4, as shown in Figure 19.

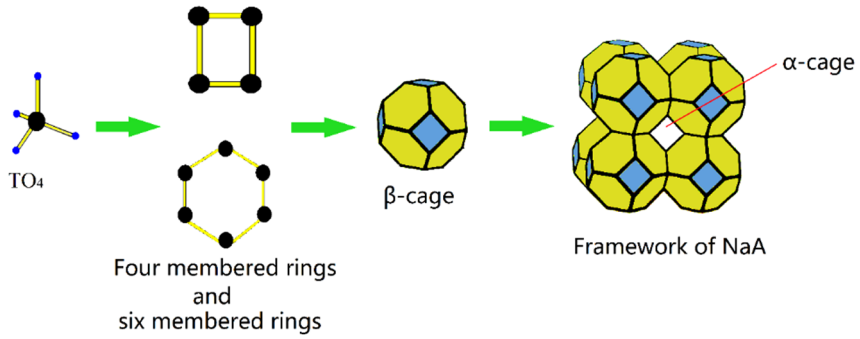

Figure 19. The formation process of NaA zeolite.

As the hydrothermal reaction continues, the TO_4 in the reaction system is connected through oxygen atoms, and the tetrahedrons formed are connected through an oxygen bridge to form a ring; four tetrahedrons make up a four-membered ring and six tetrahedrons make up a six-membered ring (the oxygen atoms are omitted, Figure 19) [40]. These rings are reduced to quadrangles and hexagons, and each of them have a Si or Al ion at the tip of the corner. Under the action bridging of cations, silicon and aluminum ions in the rings are further condensed around cations and continue to connect in three-dimensional space to form β cages (Figure 19). The β cage is a chamfered octahedron containing 6 four-membered rings; 8 six-membered rings; and 24 angular apex, β-cages arranged in the form of body-centered cubes, which are connected by a double quaternion ring, resulting in an α cage (Figure 19) and a three-dimensional skeleton structure at the center of the cell.

When the cages are formed, they will continue to form the zeolite cages; the zeolite cages will continue to expand in a three-dimensional direction according to the body-centered cubic structure. When there has been a certain amount of expansion, they will generate a certain geometric shape of the grain. The little grain seeds continue to grow in the hydrothermal system and finally form NaA zeolite crystals.

4. Conclusions

Through this study, these conclusions are drawn as follows:

(1) Calcination of the coal gangue at 700 °C for 2 h and then leaching the calcined powder by 20% hydrochloric acid; the liquid to solid ratio is 3:1 at 90 °C for 7 h and can remove most of the iron ions.

(2) Evenly mixing the sodium carbonate with the acid-leached filter residue according to the mass ratio of m(acid leached residue): m(sodium carbonate) = 1:1.1, the mixture is melted at 750 °C for 2 h, then acid-leached filter residue turns into $NaAlSiO_4$; the rests are amorphous SiO_2 and Al_2O_3, which both have high chemical activity and can participate in the crystallization reaction, so the acid-leached filter residue is activated absolutely.

(3) $n(SiO_2)/n(Al_2O_3) = 2.0$, $n(Na_2O)/n(SiO_2) = 2.1$, $n(H_2O)/n(Na_2O) = 55$, aging at 60 °C for 2 h, and crystallization at 94 °C for 4 h are the optimized conditions for NaA zeolite synthesis.

Compared with [41,42], the preparation conditions obtained in this study are more mild, the purity of the product is higher, and there are no impurity crystals in the product.

Author Contributions: D.K.: conceptualization, writing—original draft, investigation, methodology, data curation. R.J.: methodology, writing-reviewing, editing and supervision. All authors have read and agreed to the published version of the manuscript.

Funding: The study is financially supported by Guizhou Provincial Education Department's Scientific and Technological Innovation Team Project (NO. [2017] 054), Guizhou Science and Technology Foundation Project (NO. [2018] 1142), and Liupanshui City Science and Technology Foundation (NO. 52020-2019-05-17).

Institutional Review Board Statement: Not applicable.

Informed Consent Statement: Not applicable.

Data Availability Statement: Not applicable.

Conflicts of Interest: The authors declare no conflict of interest.

References

1. Niu, X.; Guo, S.; Gao, L.; Cao, Y.; Wei, X. Mercury release during thermal treatment of two coal gangues and two coal slimes under N_2 and in air. *Energy Fuels* **2017**, *31*, 8648–8654. [CrossRef]
2. Xu, H.; Song, W.; Cao, W.; Gang, S.; Lu, H.; Yang, D.; Chen, D.; Zhang, R. Utilization of coal gangue for the production of brick. *J. Mater. Cycles Waste Manag.* **2016**, *19*, 1270–1278. [CrossRef]
3. Du, H.; Ma, L.; Liu, X.-Y.; Zhang, F.; Yang, X.; Wu, Y.; Zhang, J. A novel mesoporous SiO_2 material with MCM-41 structure from coal gangue: Preparation, ethylenediamine modification, and adsorption properties for CO_2 capture. *Energy Fuels* **2018**, *32*, 5374–5385. [CrossRef]
4. Liu, M.; Zhu, Z.; Zhang, Z.; Chu, Y.; Yuan, B.; Wei, Z. Development of highly porous mullite whisker ceramic membranes for oil-in-water separation and resource utilization of coal gangue. *Sep. Purif. Technol.* **2020**, *237*, 116483. [CrossRef]
5. Zhao, H.; Chen, Y.; Duan, X. Study on the factors affecting the deep reduction of coal gangue containing high contents of iron and sulfur. *Fuel* **2020**, *288*, 119571. [CrossRef]
6. Ma, H.; Zhu, H.; Wu, C.; Chen, H.; Sun, J.; Liu, J. Study on compressive strength and durability of alkali-activated coal gangue-slag concrete and its mechanism. *Powder Technol.* **2020**, *368*, 112–124. [CrossRef]
7. Xiao, M.; Ju, F.; He, Z. Research on shotcrete in mine using non-activated waste coal gangue aggregate. *J. Clean. Prod.* **2020**, *259*, 120810. [CrossRef]
8. Du, T.; Wang, D.; Bai, Y.; Zhang, Z. Optimizing the formulation of coal gangue planting substrate using wastes: The sustainability of coal mine ecological restoration. *Ecol. Eng.* **2020**, *143*, 105669. [CrossRef]
9. Jouni, R.; Katja, O.; Paivo, K.; Marcello, R.; Mirja, I. Milling of peat-wood fly ash: Effect on water demand of mortar and rheology of cement paste. *Constr. Build. Mater.* **2018**, *180*, 143–153.
10. Zhou, C.; Liu, G.; Wu, S.; Lam, P.K.S. The environmental characteristics of usage of coal gangue in bricking-making: A case study at Huainan, China. *Chemosphere* **2014**, *95*, 274–280. [CrossRef]
11. Yang, Z.; Zhang, Y.; Liu, L.; Seshadri, S.; Wang, X.; Zhang, Z. Integrated utilization of sewage sludge and coal gangue for cement clinker products: Promoting tricalcium silicate formation and trace elements immobilization. *Materials* **2016**, *9*, 275. [CrossRef]
12. Han, J.; Jin, X.; Song, C.; Bi, Y.; Liu, Q.; Liu, C.; Ji, N.; Lu, X.; Ma, D.; Li, Z. Rapid synthesis and NH3-SCR activity of SSZ-13 zeolite via coal gangue. *Green Chem.* **2019**, *22*, 219–229. [CrossRef]
13. Chen, J.; Lu, X. Synthesis and characterization of zeolites NaA and NaX from coal gangue. *J. Mater. Cycles Waste Manag.* **2017**, *20*, 489–495. [CrossRef]
14. Jin, Y.; Li, L.; Liu, Z.; Zhu, S.; Wang, D. Synthesis and characterization of low-cost zeolite NaA from coal gangue by hydrothermal method. *Adv. Powder Technol.* **2021**, *32*, 791–801. [CrossRef]
15. Wang, X.; Zhang, Y. Synthesis and characterization of zeolite A obtained from coal gangue for the adsorption of F^- in wastewater. *Sci. Adv. Mater.* **2019**, *11*, 277–282. [CrossRef]
16. Ren, J.; Xie, C.; Guo, X.; Qin, Z.; Lin, J.; Li, Z. Combustion characteristics of coal gangue under an atmosphere of coal mine methane. *Energy Fuels* **2012**, *28*, 3688–3695. [CrossRef]
17. Merrikhpour, H.; Jalali, M. Comparative and competitive adsorption of cadmium, copper, nickel, and lead ions by iranian natural zeolite. *Clean. Technol. Environ. Policy* **2013**, *15*, 303–316. [CrossRef]
18. Polat, E.; Karaca, M.; Demir, H.; Onus, A.N. Use of natural zeolite (clinoptilolite) in agriculture. *J. Fruit Ornam. Plant Res.* **2004**, *12*, 183–189.
19. Muzic, M.; Sertic-Bionda, K.; Adzamic, T. Evaluation of commercial adsorbents and their application for desulfurization of model fuel. *Clean. Technol. Environ. Policy* **2012**, *14*, 283–290. [CrossRef]
20. Zhu, J.; Meng, X.; Xiao, F. Mesoporous zeolites as efficient catalysts for oil refining and natural gas conversion. *Front. Chem. Sci. Eng.* **2013**, *7*, 233–248. [CrossRef]
21. Yilmaz, B.; Müller, U. Catalytic applications of zeolites in chemical industry. *Top. Catal.* **2009**, *52*, 888–895. [CrossRef]
22. Qian, T.; Li, J. Synthesis of Na-A zeolite from coal gangue with the in-situ crystallization technique. *Adv. Powder Technol.* **2015**, *26*, 98–104. [CrossRef]
23. Lu, X.; Shi, D.; Chen, J. Sorption of Cu^{2+} and Co^{2+} using zeolite synthesized from coal gangue: Isotherm and kinetic studies. *Environ. Earth Sci.* **2017**, *76*, 591. [CrossRef]

24. Li, H.; Zheng, F.; Wang, J.; Zhou, J.; Huang, X.; Chen, L.; Hu, P.; Gao, J.; Zhen, Q.; Bashir, S.; et al. Facile preparation of zeolite-activated carbon composite from coal gangue with enhanced adsorption performance. *Chem. Eng. J.* **2020**, *390*, 124513. [CrossRef]
25. Jha, B.; Singh, D.N. A three step process for purification of fly ash zeolites by hydrothermal treatment. *Appl. Clay Sci.* **2014**, *90*, 122–129. [CrossRef]
26. Khaleque, A.; Alam, M.; Hoque, M.; Mondal, S.; Bin Haider, J.; Xu, B.; Johir, M.; Karmakar, A.K.; Zhou, J.; Ahmed, M.B.; et al. Zeolite synthesis from low-cost materials and environmental applications: A review. *Environ. Adv.* **2020**, *2*, 100019. [CrossRef]
27. Belviso, C.; Cavalcante, F.; Niceforo, G.; Lettino, A. Sodalite, faujasite and A-type zeolite from 2:1dioctahedral and 2:1:1 trioctahedral clay minerals. A singular review of synthesis methods through laboratory trials at a low incubation temperature. *Powder Technol.* **2017**, *320*, 483–497. [CrossRef]
28. Ayele, L.; Perez-Pariente, J.; Chebude, Y.; Diaz, I. Conventional versus alkali fusion synthesis of zeolite A from low grade kaolin. *Appl. Clay Sci.* **2016**, *132*, 485–490. [CrossRef]
29. Bi, H.; Wang, C.; Lin, Q.; Jiang, X.; Jiang, C.; Bao, L. Combustion behavior, kinetics, gas emission characteristics and artificial neural network modeling of coal gangue and biomass via TG-FTIR. *Energy* **2020**, *213*, 118790. [CrossRef]
30. Han, J.; Ha, Y.; Guo, M.; Zhao, P.; Liu, Q.; Liu, C.; Song, C.; Ji, N.; Lu, X.; Ma, D.; et al. Synthesis of zeolite SSZ-13 from coal gangue via ultrasonic pretreatment combined with hydrothermal growth method. *Ultrason. Sonochemistry* **2019**, *59*, 104703. [CrossRef] [PubMed]
31. Eilertsen, E.A.; Nilsen, M.H.; Wendelbo, R.; Olsbye, U.; Lillerud, K.P. Synthesis of high silica CHA zeolites with controlled Si/Al ratio. *Stud. Surf. Sci. Catal.* **2008**, *174*, 265–268.
32. Wang, Q.; Wang, L.; Wang, H.; Li, Z.; Zhang, X.; Zhang, S.; Zhou, K. Effect of SiO_2/Al_2O_3 ratio on the conversion of methanol to olefins over molecular sieve catalysts. *Front. Chem. Sci. Eng.* **2011**, *5*, 79–88. [CrossRef]
33. Kosinov, N.; Auffret, C.; Borghuis, G.J.; Sripathi, V.; Hensen, E. Influence of the si/al ratio on the separation properties of SSZ-13 zeolite membranes. *J. Membr. Sci.* **2015**, *484*, 140–145. [CrossRef]
34. Li, J.; Zhang, Z.; Li, X.; Bao, S.; Liu, L.; He, H.; Lai, X.; Zhang, L.; Zhang, P. Preparation of ZSM-5 molecular sieve by diatomaceous earth in-situ crystallization. *Integr. Ferroelectr.* **2018**, *189*, 165–174. [CrossRef]
35. Yao, G.; Lei, J.; Zhang, X.; Sun, Z.; Zheng, S. One-step hydrothermal synthesis of zeolite X powder from natural low-grade diatomite. *Materials* **2018**, *11*, 906. [CrossRef]
36. Maia, A.Á.B.; Dias, R.N.; Angélica, R.S.; Neves, R.F. Influence of an aging step on the synthesis of zeolite NaA from brazilian amazon kaolin waste. *J. Mater. Res. Technol.* **2019**, *8*, 2924–2929. [CrossRef]
37. Guo, Y.P.; Lee, N.H.; Oh, H.-J.; Yoon, C.R.; Rhee, C.K.; Lee, K.S.; Kim, S.J. Fabrication of oriented TiO_2 based nanotube array thin films. *Solid State Phenom.* **2008**, *135*, 19–22. [CrossRef]
38. Behin, J.; Bukhari, S.S.; Kazemian, H.; Rohan, S. Developing a zero liquid discharge process for zeolitization of coal fly ash to synthetic NaP zeolite. *Fuel* **2016**, *7*, 195–202. [CrossRef]
39. Bukhari, S.S.; Behin, J.; Kazemian, H.; Rohani, S. A comparative study using direct hydrothermal and indirect fusion methods to produce zeolites from coal fly ash utilizing single-mode microwave energy. *J. Mater. Sci. Lett.* **2014**, *49*, 8261–8271. [CrossRef]
40. Bu, N.; Liu, X.; Song, S.; Liu, J.; Yang, Q.; Li, R.; Zheng, F.; Yan, L.; Zhen, Q.; Zhang, J. Synthesis of NaY zeolite from coal gangue and its characterization for lead removal from aqueous solution. *Adv. Powder Technol.* **2020**, *31*, 2699–2710. [CrossRef]
41. Li, Y.; Peng, T.; Man, W.; Ju, L.; Zheng, F.; Zhang, M.; Guo, M. Hydrothermal synthesis of mixtures of NaA zeolite and sodalite from Ti-bearing electric arc furnace slag. *RSC Adv.* **2016**, *6*, 8358–8366. [CrossRef]
42. Su, Q.; He, Y.; Yang, S.; Wan, H.; Cui, X. Synthesis of NaA-zeolite microspheres by conversion of geopolymer and their performance of Pb (II) removal. *Appl. Clay Sci.* **2020**, *20*, 105914. [CrossRef]